

DOI: 10.1002/adem.201200246

## Multiple Memory Shape Memory Alloys\*\*

By Mohammad Ibraheem Khan, Andrew Pequegnat\* and Y. Norman Zhou\*

*Until now, shape memory alloys (SMAs) have been largely limited to “remembering” a single memory. In other words, monolithic components only possess a single set of functional properties. The current work describes how theorized change to local chemical composition induced through laser processing enables controlled augmentation of transformation temperatures. Proof of concept was demonstrated by locally embedding multiple shape memories into a monolithic NiTi component. This novel technique overcomes traditional fabrication challenges and promises to enhance SMA functionality and facilitate novel applications through producing a new class of smart materials; namely multiple memory materials (MMMs).*

The unique capabilities of shape memory alloys (SMAs) have made them ideal engineering materials for novel devices currently implemented in numerous industries including medical, automotive, aerospace, and micro-electronics. Their potential in high profile applications such as non-invasive surgical tools, biomedical implants, and energy harvesting clean technologies are driving innovation and application of these smart materials.<sup>[1–3]</sup> Among all SMAs, NiTi alloys are the most commonly applied due to superior strength, ductility, recoverable strains, corrosion resistance, biocompatibility, and stability of transformation temperatures.

The functional properties of SMAs, namely the shape memory effect and pseudoelasticity, are attributed to a reversible thermoelastic austenite-martensite phase transfor-

mation. As a result, these functional properties are closely linked to phase transformation temperatures.<sup>[4,5]</sup> The high sensitivity of transformation temperatures to alloy composition and processing history<sup>[6–9]</sup> has made efforts to create application-specific alloys problematic. Furthermore, traditional SMA fabrication technologies are performance limiting since monolithic components consist of only a single set of phase transformation characteristics. A novel material processing protocol is therefore required to overcome these challenges to enable further innovation and application.

In the past, various techniques have been applied to SMAs in attempts to control local functionality. Specific methods previously attempted included, direct electric resistance heat treatment (DERHT),<sup>[10,11]</sup> direct hot air heat treatment (DHAHT),<sup>[10]</sup> powder metallurgy (PM),<sup>[12–15]</sup> gradient annealing,<sup>[16]</sup> laser annealing,<sup>[17]</sup> and joining of multiple alloys.<sup>[18]</sup> All of these techniques aimed to enable designs that utilize more than one set of functional properties in a monolithic component. However, inherent processing issues restricted their widespread application. For example, local heat treatment methods can only be applied to simple geometries, are time intensive, and provide a lack of resolution in functional properties.<sup>[10,11,16,17]</sup> PM methods exhibited issues with porosity, poor surface finish, and composition inhomogeneity leading to undesirable intermetallic compound (IMC) formation.<sup>[13–15]</sup> In contrast, joining of multiple alloys showed to be relatively effective for simple devices.<sup>[18]</sup> However, challenges associated with joining dissimilar SMAs (i.e., IMC formation) and more complex designs again limit application. Hence, past attempts at achieving multiple functional properties in a single component have not been successful. A rapid processing protocol is still required that is capable of high resolution and avoids the aforementioned issues.

The current article presents a novel laser processing technique that locally augments transformation temperatures

[\*] Dr. M. I. Khan

Smarter Alloys, Inc., MaRS Centre, South Tower, 101 College Street, Suite 200, Toronto, ON M5G 1L7, Canada

E-mail: [ibraheem@smarteralloys.com](mailto:ibraheem@smarteralloys.com)

A. Pequegnat, Prof. Y. N. Zhou

Centre for Advanced Materials Joining (CAMJ), University of Waterloo, 200 University Avenue West, Waterloo, ON N2L 3G1, Canada

E-mail: [apeekugn@uwaterloo.ca](mailto:apeekugn@uwaterloo.ca); [nzhou@uwaterloo.ca](mailto:nzhou@uwaterloo.ca)

A. Pequegnat, Prof. Y. N. Zhou

Centre for Bioengineering and Biotechnology (CBB), University of Waterloo, 200 University Avenue West, Waterloo, ON N2L 3G1, Canada

[\*\*] The Authors would like to acknowledge the support of the Natural Sciences and Engineering Research Council of Canada (NSERC). Also, a special thanks to Siu Kei Tang, Billy Tam, Matt Daly, and Jeff Wang of the microwelding subgroup of the Centre for Advanced Materials Joining (CAMJ).

Supporting Information is available from the Wiley Online Library or from the author.

of SMAs. Specifically, theorized change to local chemical composition via controlled vaporization was implemented to modify the Ni:Ti ratio in the binary NiTi system. Remarkably, this work resulted in proof of concept by successfully embedding multiple memories in a monolithic NiTi component. This was achieved with the necessary resolution, while avoiding detrimental defects observed in competing technologies. This unprecedented technique overcomes traditional fabrication challenges while enabling the realization of a new class of smart materials known as multiple memory materials (MMMs).

## 1. Results and Discussion

### 1.1. The Vaporization Concept

Composition changes induced by vaporization using high power density processing methods (e.g., laser beam, electron beam, etc.) is well documented in literature.<sup>[19–27]</sup> Prior studies have concluded that local loss of elemental constituents can be detrimental to the properties of a bulk material. For example, it has been reported that the loss of certain alloying elements during laser processing was responsible for reduction in solid solution strengthening in Al alloys (i.e., due to loss of Mg)<sup>[20,23]</sup> or decreased corrosion resistance in stainless steels (i.e., due to loss of Cr).<sup>[22,24–27]</sup> The concept of utilizing laser induced vaporization as an advantage has not yet been investigated. However, by controlling elemental loss during laser processing, the local properties of an alloy can theoretically be precisely tailored for that of a specific application. NiTi SMAs are a prime example of a group of materials that are extremely sensitive to change in composition, where the advantages of elemental loss during processing can be realized. Slight modifications to composition have been shown to substantially alter transformation temperatures which play a critical role in their functional properties. For example, composition changes of 1 at.% have been reported to result in an 80–100 K change in transformation temperatures of a binary NiTi SMA.<sup>[8,9,28]</sup> Similarly, transformation temperatures and temperature/stress hysteresis in ternary (or quaternary, etc.) NiTi systems and other SMAs, such as Cu–Al alloys, were also found to be highly composition dependent.<sup>[29–36]</sup> A laser induced controlled vaporization protocol is therefore proposed for quickly modifying the local functional properties of monolithic SMA components.

### 1.2. Selective Vaporization of Elemental Constituents

To apply this novel vaporization protocol to NiTi SMAs it is necessary to determine the relative vaporization flux of each elemental constituent (i.e., Ni and Ti) to aid in predicting the change in composition. The relative loss of elemental constituents during laser processing is determined largely by their volatility.<sup>[19–27]</sup> More specifically, the pressure gradient has been shown to have the largest effect on vaporization flux during laser processing.<sup>[26,27]</sup> Therefore, relative loss of elemental constituents was approximated by calculating the

vapor pressures of each element. Assuming ideal conditions at high temperatures, equilibrium vapor pressure of both Ni and Ti can be calculated over the alloy mixture of the molten pool via Equation (1):<sup>[25,26]</sup>

$$P_i = X_i P_i^0 \quad (1)$$

where  $X_i$  is the mole fraction of the element  $i$  and  $P_i^0$  is the equilibrium vapor pressure of the element  $i$  over pure  $i$ . The equilibrium pressure  $P_i^0$  of each alloying element was calculated with respect to temperature using Equation (2):<sup>[37]</sup>

$$\log_{10}(P_i^0) = A + \frac{B}{T} + C \log_{10}(T) + DT + ET^2 \quad (2)$$

where  $A, B, C, D$ , and  $E$  are constant coefficients and  $T$  refers to temperature. The corresponding coefficients for Ni and Ti that were used in this study are provided in Table 1.<sup>[37]</sup>

Calculated vapor pressures of Ni and Ti over an equiatomic NiTi alloy as a function of temperature are presented in Figure 1. Significant differences in vapor pressures were observed between the two elemental constituents, with Ni being substantially larger over the plotted temperature range.

Table 1. Constant coefficients for calculation of equilibrium vapor pressure ( $P_i^0$ ) of Ni and Ti.<sup>[37]</sup>

	A	B	C	D	E
Ni	−214.3	−3.52E + 03	7.49E + 01	−1.80E−02	1.51E−06
Ti	−194.8742	−8.27E + 03	6.83E + 01	−1.73E−02	1.55E−06

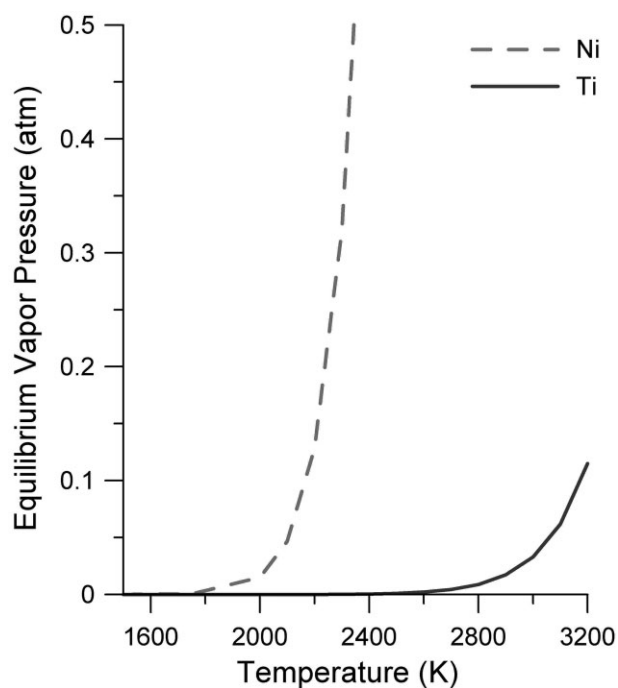


Fig. 1. Nickel and Titanium vapor pressures over an equiatomic NiTi mixture. Significantly higher vapor pressure of Nickel corresponds to a comparatively larger vaporization flux.

Hence, the vaporization flux of Ni can be expected to be larger than that of Ti during laser processing of a near equiatomic NiTi SMA; the basis of the controlled constituent vaporization protocol developed in this work.

### 1.3. Augmentation of Transformation Temperatures

A decrease in the Ni:Ti ratio translates to an increase in phase transformation temperatures.<sup>[8,9,38–41]</sup> Therefore, the anticipated loss of Ni following laser processing was expected to increase the phase transformation temperatures; as was found by Meier *et al.*, studying selective laser melting of NiTi.<sup>[42]</sup> This hypothesis agrees with results from the differential scanning calorimetry (DSC) analysis presented in Figure 2. After processing the NiTi alloy, a second set of transformation peaks appeared at higher temperatures compared to those of the solutionized base metal. Furthermore, during pulsed Nd:YAG laser processing it has been shown that vaporization primarily occurs during the first few milliseconds of laser application, when utilizing the keyhole laser interaction mode.<sup>[27]</sup> Therefore, a compound effect resulted when using multiple pulses that maximized vaporization. Accordingly, transformation temperatures were found to increase with each additional laser pulse, identifying the possibility for high resolution through this laser processing protocol (Figure 2).

Relative composition change of laser processed materials is highly dependent on a balance between the vaporization flux of elemental constituents and molten pool dilution.<sup>[26,27]</sup> Since vaporization flux and molten pool dilution are closely linked to laser processing parameters, it was of interest to investigate the effects of peak power and pulse duration on the compositionally sensitive transformation temperatures. Peak power and pulse duration, however, were found to have only a minor effect compared to the number of applied laser pulses.

Effects of pulse duration on transformation temperatures are shown in Figure 3. Using a laser power of 0.6 kW, increasing pulse duration increased DSC peak intensity. The more prominent transformation peaks were a result of an increase in the processed material to base metal volume ratio with increased pulse duration. Transformation temperatures of processed material decreased slightly (i.e., by <20 K) with increasing pulse duration, as shown in Figure 4. Since vaporization flux is highest during the first few milliseconds of the laser pulse and decreases drastically with pulse duration,<sup>[27]</sup> dilution of the molten pool caused by an increase in volume was likely the mechanism behind decreasing transformation temperatures with longer pulse durations. Hence, vaporization flux decreased and the pool volume increased with increased pulse duration, leading to smaller changes in final composition; consistent with literature.<sup>[27]</sup>

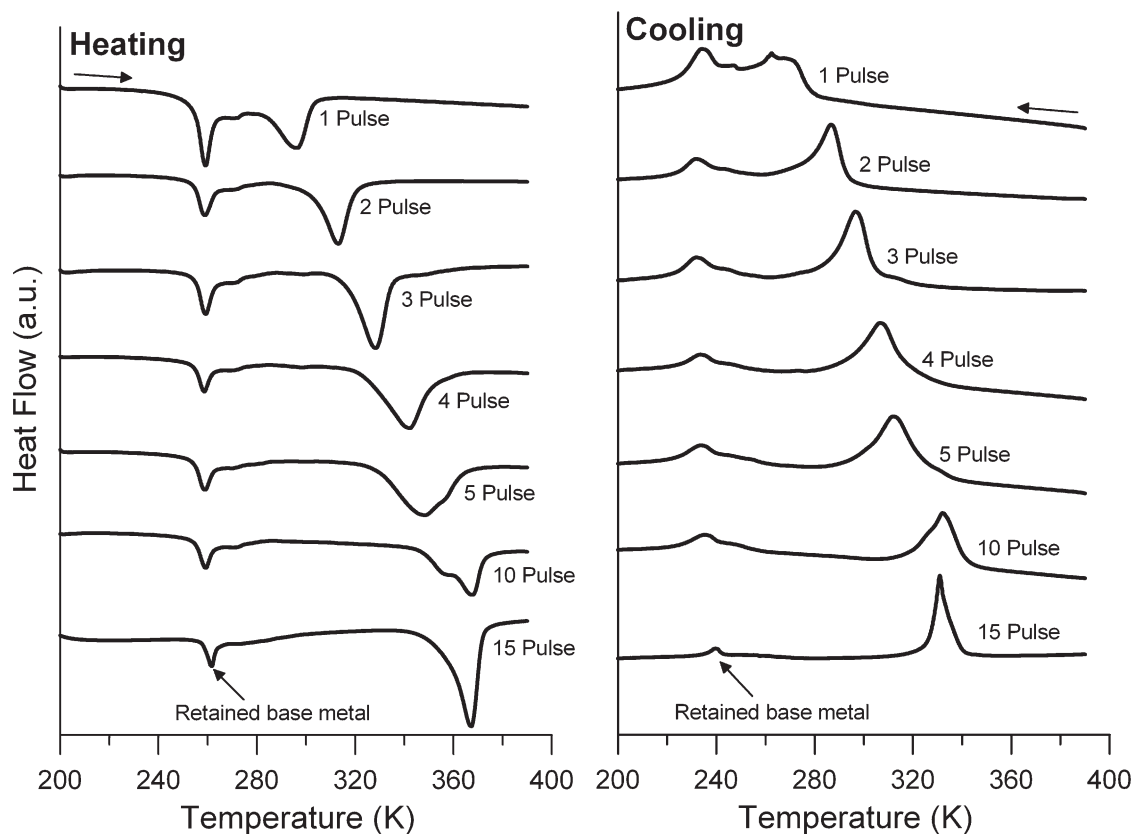


Fig. 2. Thermo-analytical DSC analysis. Following laser processing with 0.6 kW peak power and 30 ms pulse duration, a second set of phase transformation peaks were identified at higher temperatures. During heating, the endothermic B2 austenite peaks were measured. Similarly, the exothermic B19' martensite peaks were measured during cooling. Increasing the number of pulses caused a compound vaporization effect, raising the transformation temperatures with increasing number of pulses.

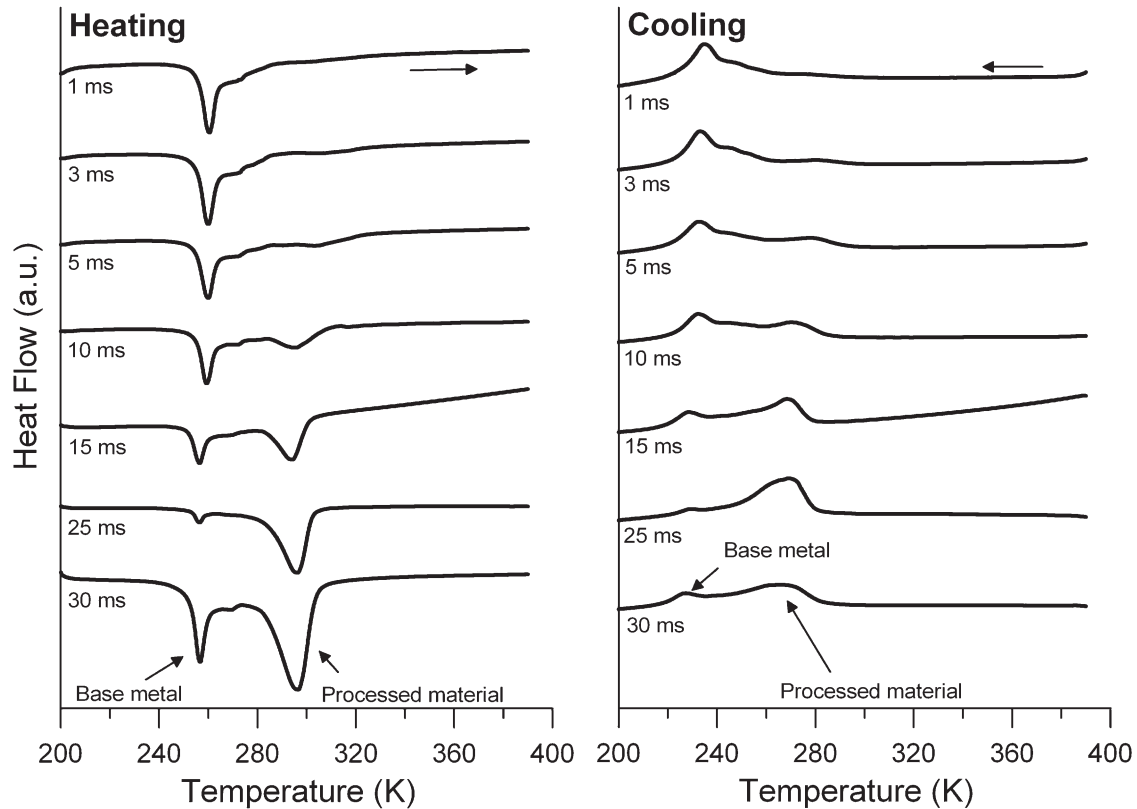


Fig. 3. The effect of pulse duration on transformation temperatures as measured by DSC analysis. Less significant changes in transformation temperature of the processed region were observed with increasing pulse duration and a laser power of 0.6 kW compared to number of laser pulses.

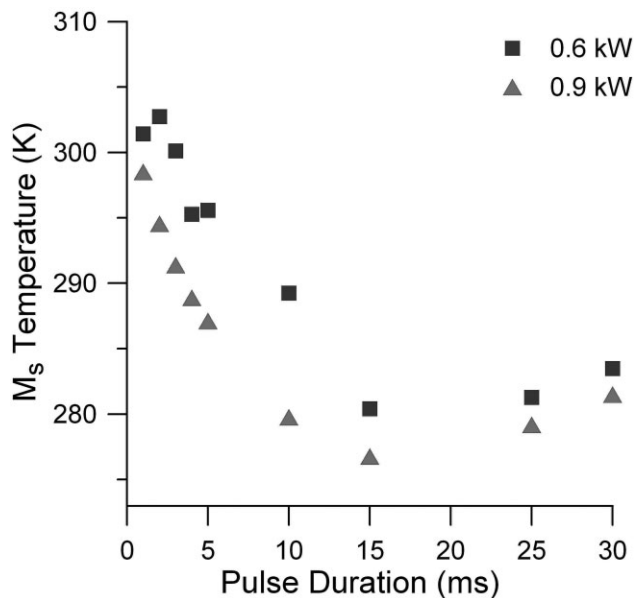


Fig. 4. Effect of laser power on transformation temperatures.  $M_s$  temperature versus pulse duration for the 0.6 and 0.9 kW laser power conditions. Less than 10 K difference in transformation temperatures was observed between the 0.6 and 0.9 kW laser power conditions.

The effects of laser power on transformation temperatures are shown in Figure 4. Only a small decrease in transformation temperature (i.e., <10 K) was observed when increasing laser power to 0.9 kW from 0.6 kW. Similar to the decrease in transformation temperatures with increasing pulse duration, increasing the laser power can also cause an increase in dilution of the molten pool leading to lower transformation temperatures.

The observed correlations between laser parameters and transformation temperatures accentuate the controllability of the process. Even though the number of pulses has the greatest effect on changes in transformation temperatures, the laser power and pulse duration are necessary to achieve application specific properties and the highest possible resolution of the process. Using multiple pulses having different power and pulse duration parameters or by using unique temporal profiles, local phase transformation characteristics can be precisely selected.

#### 1.4. Verification of the Vaporization Mechanism

Thus far thermoanalytical DSC analysis was shown to be a useful tool in identifying the effects of laser parameters on transformation temperatures. However, it is still necessary to definitively confirm that vaporization was in fact the primary mechanism at play.

There have been some inconsistencies in prior studies that investigated the effects of composition on transformation temperatures.<sup>[38–40]</sup> However, investigators have consistently reported that when the composition of solutionized NiTi alloys was near or below equiatomic, the maximum  $M_s$  temperature is approximately 338 K (65 °C).<sup>[8,9]</sup> When Ni composition is below 49 at.%, transformation temperatures become independent of composition due to Ti saturation. The  $M_s$  transformation temperatures plotted with respect to the number of laser pulses in Figure 5 shows a steady increase until the 338 K (65 °C) maximum  $M_s$  temperature was achieved. This suggests that with increasing number of pulses a threshold exists where the processed material becomes Ti-rich. Therefore, these DSC results strongly correlate the augmentation of transformation temperature to a decrease in Ni:Ti ratio.

Compositional and phase analysis further confirmed that changes in local chemistry were the primary mechanism behind the altered transformation temperatures. An energy-dispersive X-ray spectroscopy (EDS) line scan including the base metal and processed region (i.e., after five laser pulses) was performed in order to detect Ni depletion as shown in Figure 6(a). Average base metal Ni content ( $50.07 \pm 0.53$  at.% Ni) was significantly higher when compared to the processed material ( $48.36 \pm 0.84$  at.% Ni). Furthermore, EDS analysis performed on the captured plume produced during laser processing showed 75.5 at.% Ni and 24.5 at.% Ti; confirming the expected higher Ni vaporization flux compared to that of Ti. The thermo-analytical DSC results were also verified using room temperature micro-X-ray diffraction (XRD); shown in Figure 6(b). Diffraction patterns of the processed region were

found to be consistent with monoclinic B19' martensite, whereas the adjacent base metal possessed the anticipated cubic B2 austenite crystal structure. This phenomenon resulted from the austenite phase being thermodynamically stable in the base metal and the martensite phase being stable in the processed region at room temperature; consistent with DSC analysis in Figure 2. Transmission electron microscopy (TEM) revealed nodular particles surrounded by a twinned martensite matrix in the processed material [Figure 6(c)]. EDS analysis identified the particles as the  $Ti_2Ni$  intermetallic; detecting Ti and Ni atomic compositions of 66.3 and 33.6 at.%, respectively. The presence of the Ti-rich  $Ti_2Ni$  intermetallic was further evidence of the compositional change of the processed alloy, since Ti was no longer soluble in NiTi. Significant amounts of Ti-rich IMCs were only found in over-processed samples where Ti saturation had occurred.

Other possible mechanisms responsible for changes in transformation temperatures in NiTi alloys include changes in dislocation density and growth of Ni-rich precipitates.<sup>[11,5,29,43]</sup> However, lower energy density laser processes that induce melting but limit vaporization lead to decreases in the transformation temperatures of binary NiTi alloys.<sup>[44]</sup> The melting of the NiTi alloy eliminates the effects of all previous processing by annihilation of dislocations and dissolution of Ni-rich precipitates. The presence of high density dislocations and Ni-rich precipitates were also not observed during TEM analysis in this work. Hence, vaporization was the primary mechanism behind the augmentation of transformation temperatures observed in this study.

### 1.5. Multiple Memory Material Proof of Concept

MMMs fabricated using this controlled constituent vaporization protocol have great potential in aiding in the realization and development of novel SMA devices. Proof of concept was demonstrated through the local modification of the transformation temperatures in the NiTi component shown in Figure 7. Commercially available material that exhibits a single set of transformation temperatures (i.e., single shape memory) was locally processed yielding processed regions with surface morphology similar to that of a pulsed laser weld, as illustrated in Figure 7(a). Pulsed Nd:YAG laser processing at the annotated sites caused a localized increase in phase transformation temperatures while the phase transformation dynamics in the untreated regions remained unchanged. This increase in transformation temperatures allowed for a two-stage (i.e., two-memory) actuation through sequential heating of the specimen beyond the austenite finish temperatures of the base metal and the processed material, respectively. A schematic and photograph of the actuation process are shown in Figure 7(b) and (c). At low temperatures the entire sample was in the martensitic phase and easily deformed (i.e., by detwinning) into a “C-like” shape. Upon heating to a temperature greater than  $T_1$ , the bulk unprocessed base metal transforms to austenite and recovers its original shape, while the processed regions remain in the martensite

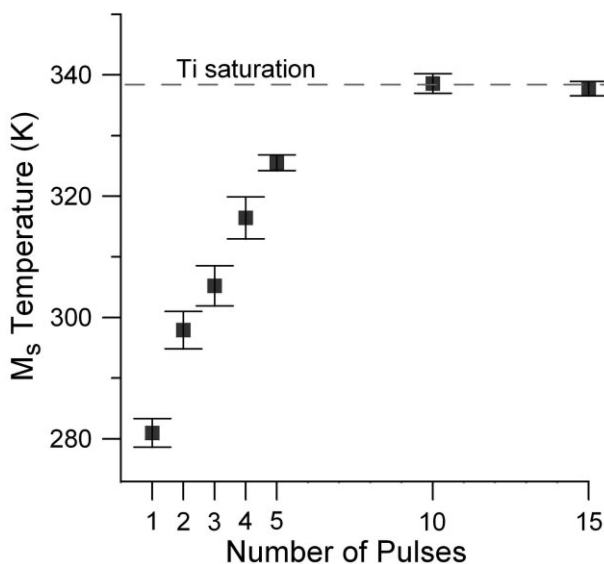


Fig. 5. Martensite start ( $M_s$ ) temperature plotted against number of laser pulses. A maximum  $M_s$  of approximately 338 K (65 °C) was achieved with increasing pulses. This maximum  $M_s$  temperature was a result of the limited solubility of Ti in NiTi below equiatomic composition. The error bars represent one standard deviation of a 6 sample population.

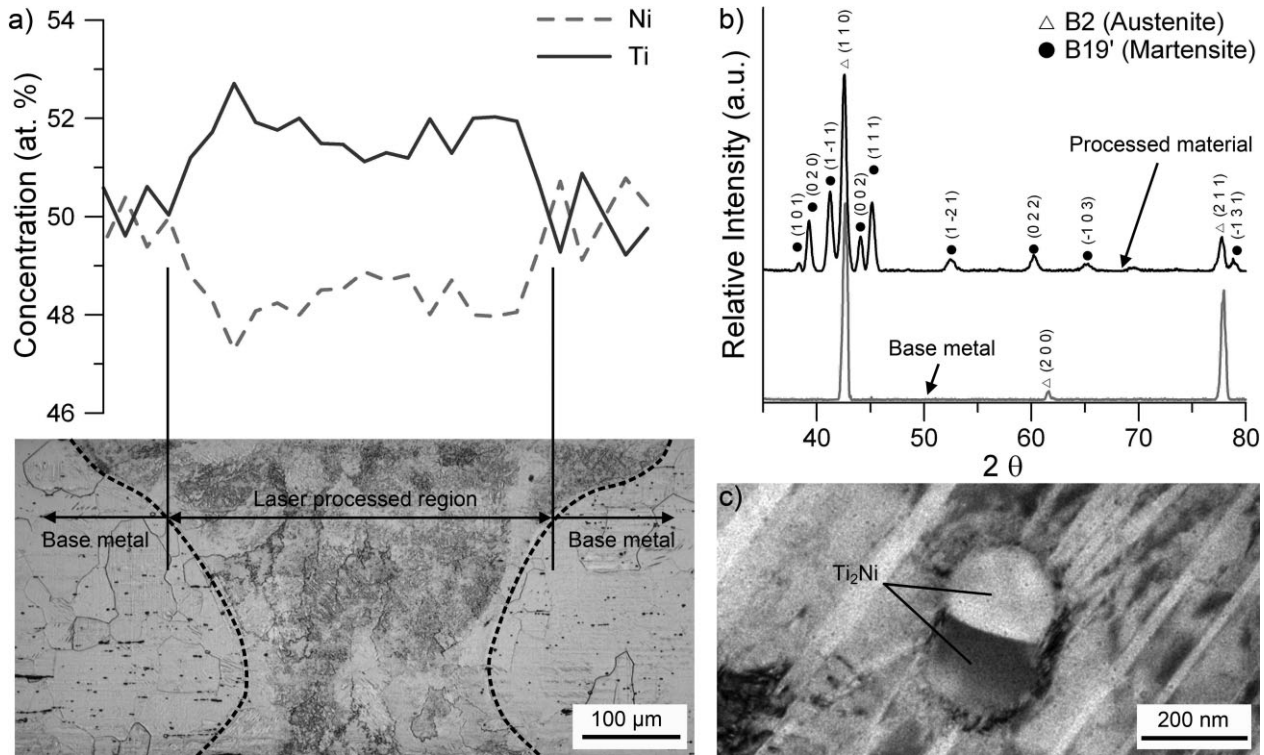


Fig. 6. Compositional and phase analysis of laser processed NiTi. (a) EDS line scan across laser processed region. A decrease in the Ni:Ti ratio was measured in the processed region (i.e., after five laser pulses) compared to the adjacent base metal resulting from the preferential vaporization of Nickel. (b) Room temperature micro-XRD analysis identified the B19' martensite phase in the processed region and the B2 austenite phase in the adjacent base metal. As a result of the local change in composition, both martensite in the processed region and austenite in the base metal were stable at room temperature in the monolithic component. (c) TEM analysis identified Ti-rich Ti<sub>2</sub>Ni intermetallics in heavily processed samples (i.e., >5 pulses). The presence of Ti<sub>2</sub>Ni was a result of Ti no longer being soluble in NiTi below equiatomic composition.

phase. Subsequently, heating to above T<sub>2</sub> induces the transformation of the processed regions to austenite and the recovery of the second shape memory (see Supporting Information Video).

In addition to the demonstrated increased functionality of MMMs, there are numerous benefits compared to competing technologies. MMMs benefit from the speed and accuracy accredited to laser processing. Also, defects such as poor surface finish, porosity, and detrimental IMC formation were not found to be issues in this study. Parallel studies are underway to further characterize and understand the performance of this new class of smart materials.

## 2. Conclusions

In conclusion, local augmentation of transformation temperatures creating MMM NiTi SMAs can be achieved through controlled constituent vaporization. With an understanding of the effects of pulsed laser processing on vaporization of elemental constituents, the local transformation temperatures of SMA components can be tailored to that of a specific application. This study focused on the binary NiTi system however, the MMM technology has potential for use on other SMAs or any other material that may benefit from constituent vaporization. Synergistic vaporization and mixing

of additional alloying elements can also be achieved using laser processing on more complex alloy systems.<sup>[45]</sup> MMMs have the potential to greatly enable the engineering of complex SMA devices. SMA functionality has been immensely improved where concepts such as, but not limited to, dynamic actuation via passive atmospheric control, self-biasing monolithic actuators, and local tuning of functional properties are now feasible.

## 3. Experimental

Commercially available 0.37 mm thick SE508 Nitinol strip manufactured by Nitinol Devices and Components, Inc. was used in this study. The chemistry for this particular NiTi alloy was 55.8 wt% (50.7 at.%) Ni and 44.2 wt% (49.3 at.%) Ti with maximum oxygen and carbon contents of 0.05 wt.% and 0.02 wt.%, respectively. The as-received cold-rolled material was heat treated for 3.6 ks at 1073 K (800 °C) followed by rapid quenching to remove the effects of prior thermo-mechanical processing and ensure no R-phase was present. A dilute solution of hydrofluoric and nitric acid was used to remove a thick black oxide before laser processing.

An LW50 A Miyachi Unitek pulsed Nd:YAG laser system with a 1.06 μm wavelength, 400 μm nominal spot diameter, and a Gaussian spatial profile was used in this work. This particular system was equipped with a power monitor allowing for accurate in situ assessment of incident power output. Processing was conducted on

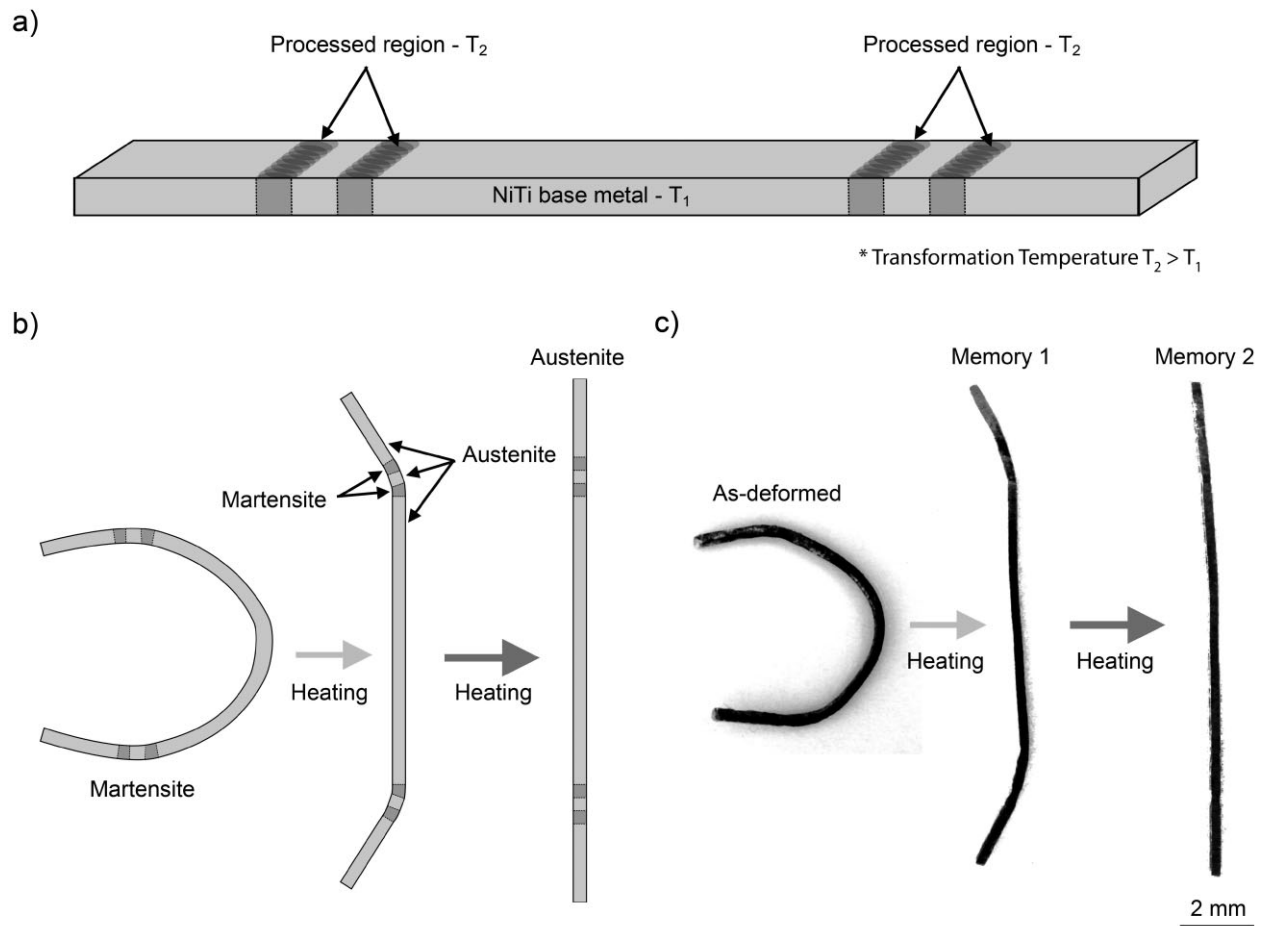


Fig. 7. MMM proof of concept. (a) Four select regions of a commercially available NiTi alloy were laser processed, increasing the phase transformation temperatures (not to scale). (b) Schematic demonstration of multiple actuations of the laser processed component. (c) Actual images of processed component during different stages of actuation. After cooling below the martensite finish temperatures of both the processed region ( $T_2$ ) and base metal ( $T_1$ ) the component was deformed by detwinning in the martensite phase to a “C-like” shape. Upon heating past the austenite phase transformation temperatures of the base metal, the base metal recovered its shape while the processed region remains strained and in the martensite phase. Further heating past the austenite transformation temperatures of the processed regions lead to a second transformation and complete recovery of the original shape of the processed NiTi component. Hence, the monolithic component possessed two distinct shape memories after processing.

monolithic NiTi sheets. The top and bottom were shielded with argon to avoid oxidation; a flow rate of  $14.2 \text{ L min}^{-1}$  (30 CFH) was found to be optimum. The minimum peak power criteria included full penetration through the NiTi strip. Peak power parameters of 0.6 and 0.9 kW with a 1 to 30 ms square pulse were used in this work.

DSC analysis was conducted using a Thermal Analysis Q2000 system equipped with a refrigerated cooling system. DSC curves were recorded in a temperature range from 198 K ( $-75^\circ\text{C}$ ) to 423 K ( $150^\circ\text{C}$ ) using a controlled heating and cooling rate of  $5 \text{ K min}^{-1}$ . The martensite start ( $M_s$ ), martensite finish ( $M_f$ ), austenite start ( $A_s$ ), and austenite finish ( $A_f$ ) phase transformation temperatures were measured using the TA Universal Analysis software (version 4.5) by calculating the intercept of the tangents to the phase transformation peak slopes and the base line; as per the ASTM F2004-05 standard. For simplification, the  $M_s$  temperature was used as a representative measure of overall transformation changes; consistent with literature. Samples were carefully extracted using a Struers, Ltd., Acutome 50 precision saw with a  $\pm 0.01 \text{ mm}$  tolerance. Due to the small specimen dimensions, remnant base metal material remained on the cut samples. Hence, transformation peaks from the base material and processed regions were measured.

Metallographic cross-sections were prepared for EDS and micro XRD analysis by polishing down to  $1 \mu\text{m}$  diamond followed by  $0.03 \mu\text{m}$  colloidal silica. Samples were etched in a 14 mL  $\text{HNO}_3$ , 3 mL HF, and 82 mL  $\text{H}_2\text{O}$  solution for 25 s to reveal microstructure.

In order to measure Ni depletion in the processed samples and analyze the composition of the vapor plume, a Jeol JSM-6460 scanning electron microscope (SEM) equipped with an INCA X-Sight 350 EDS analysis aperture was used for chemical analysis. Chemical measurements were collected at a 20 keV acquisition energy using a nominal  $1 \mu\text{m}$  interaction spot. NiTi SMA samples were polished and etched following the same procedure outlined for optical microscopy analysis. Prior to SEM analysis, the samples were carbon coated for improved conductivity. For analysis of the vapor plume, vaporized elements were collected by placing a quartz tube co-axial to the incident laser beam where vapor condensed on the inner wall. A laser peak power of 0.6 kW with 30 ms pulse duration was used for this test.

Crystallographic phases in laser processed samples were identified using XRD analysis. Room temperature XRD patterns were captured using a Rigaku SA-HF3 ( $1.54 \text{ \AA}$  Copper- $\text{K}\alpha$ ) X-ray source equipped with a  $500 \mu\text{m}$  collimator operating at an excitation voltage of 50 kV and 40 mA current.

A Philips CM12 TEM equipped with EDS and an accelerating voltage of 120 keV was used in this study. The TEM sample preparation was conducting using a Fischione ion milling system at 183 K (−90 °C) to minimize heat induced artifacts.

Received: July 13, 2012

Final Version: December 20, 2012

- [1] T. G. Frank, W. Xu, A. Cuschieri, *Minim. Invasive Ther.* **2000**, *9*, 89.
- [2] C. Smith, A. Villanueva, K. Joshi, Y. Tadesse, S. Priya, *Smart Mater. Struct.* **2011**, *20*, 012001.
- [3] A. C. Keefe, G. P. McKnight, G. A. Herrera, P. A. Bedegi, C. B. Churchill, A. L. Browne, J. Brown, in *Proceedings of the ASME 2011 Conference on Smart Materials, Adaptive Structures and Intelligent Systems*, Phoenix, Arizona **2011**, p. 669.
- [4] X. Huang, Y. Liu, *Scr. Mater.* **2001**, *45*, 153.
- [5] C. P. Frick, A. M. Ortega, J. Tyber, A. El. M. Maksound, H. J. Maier, Y. Liu, K. Gall, *Mater. Sci. Eng., A* **2005**, *405*, 34.
- [6] M. H. Wu, *Mater. Sci. Forum* **2002**, *394*, 285.
- [7] D. Miller, D. Lagoudas, *Mater. Sci. Eng., A* **2001**, *308*, 161.
- [8] J. Frenzel, E. P. George, A. Dlouhy, Ch. Somsen, M. F.-X. Wagner, G. Eggeler, *Acta Mater.* **2010**, *58*, 3444.
- [9] W. Tang, *Metall. Mater. Trans., A* **1997**, *28A*, 537.
- [10] F. Miura, M. Mogi, Y. Ohura, *Eur. J. Orthod.* **1988**, *10*, 187.
- [11] G. Airoldi, G. Riva, *J. Physique IV, Colloque C2, sup. J. Physique III* **1995**, *5*, 397.
- [12] D. Cluff, S. Corbin, R. Gorbet, in *Proceedings of Cansmart 2009, the 12th Cansmart Meeting – International Workshop on Smart Materials and Structures*, (Ed: G. Akhras), Montreal, Quebec **2009**, p. 293.
- [13] J. C. Hey, A. P. Jardine, *Mater. Sci. Eng., A* **1994**, *188*, 291.
- [14] M. Whitney, S. F. Corbin, R. B. Gorbet, *Acta Mater.* **2008**, *56*, 559.
- [15] B. Vamsi Krishna, S. Bose, A. Bandyopadhyay, *Metall. Mater. Trans., A* **2007**, *38A*, 1096.
- [16] A. S. Mahmud, Y. Liu, T. H. Nam, *Smart Mater. Struct.* **2008**, *17*, 015031.
- [17] Q. Meng, Y. Liu, H. Yang, B. S. Shariat, T. H. Nam, *Acta Mater.* **2012**, *60*, 1658.
- [18] P. Sevilla, F. Martorell, C. Libenson, J. A. Planell, F. J. Gil, *J. Mater. Sci.: Mater. Med.* **2008**, *19*, 525.
- [19] A. Block-Bolten, T. W. Eager, in *Trends in Welding Research in the United States* (Ed: S. A. David), ASM International, Novelty, OH **1982**, p. 55.
- [20] D. W. Moon, E. A. Metzbower, *Weld. J. Res. Sup.* **1983**, *62*, 53.
- [21] A. Block-Bolten, T. W. Eager, *Metall. Trans. B* **1984**, *15B*, 463.
- [22] P. A. A. Khan, T. Debroy, *Metall. Trans. B* **1984**, *15B*, 641.
- [23] A. Blake, J. Mazumder, *J. Eng. Ind.* **1985**, *107*, 275.
- [24] M. M. Collur, A. Paul, T. Debroy, *Metall. Trans. B* **1987**, *18B*, 733.
- [25] X. He, T. Debroy, P. W. Fuerschbach, *J. Phys. D: Appl. Phys.* **2003**, *36*, 3079.
- [26] X. He, T. Debroy, P. W. Fuerschbach, *J. Appl. Phys.* **2004**, *96*, 4547.
- [27] M. Jandaghi, P. Parvin, M. J. Torkamany, J. Sabbaghzadeh, *J. Phys. D: Appl. Phys.* **2008**, *41*, 235503.
- [28] X. Ren, K. Otsuka, *Mater. Sci. Forum* **2000**, 327–328, 429.
- [29] H. Funakubo, *Shape Memory Materials*, Gordon and Breach Scientific Publishers, New York, NY **1987**.
- [30] K. H. Eckelmeyer, *Scr. Metall.* **1976**, *10*, 667.
- [31] H. C. Donkersloot, J. H. N. Van Vucht, *J. Less-Common Met.* **1970**, *20*, 83.
- [32] P. G. Lindquist, C. M. Wayman, *Proc. MRS Int. Mtg. Adv. Mater.* **1989**, *9*, 123.
- [33] R. Zarnetta, R. Takahashi, M. L. Young, A. Savan, Y. Furuya, S. Thienhaus, B. Maaß, M. Rahim, J. Frenzel, H. Brunken, Y. A. Chu, V. Srivastava, R. D. James, I. Takeuchi, G. Eggeler, A. Ludwig, *Adv. Funct. Mater.* **2010**, *20*, 1917.
- [34] M. Zarinjad, Y. Liu, *Adv. Funct. Mater.* **2008**, *18*, 2789.
- [35] J. Cui, Y. S. Chu, O. O. Famodu, Y. Furuya, J. Hatrick-Simpers, R. D. James, A. Ludwig, S. Thienhaus, M. Wuttig, Z. Zhang, I. Takeuchi, *Nat. Mater.* **2006**, *5*, 286.
- [36] V. Recarte, R. B. Pérez-sáez, J. San Juan, E. H. Bocanegra, M. L. Nó, *Metall. Mater. Trans., A* **2002**, *33A*, 2581.
- [37] C. L. Yaws, *Handbook of Vapor Pressure*, Vol. 4, Gulf Publishing Co, Houston, TX **1995**.
- [38] F. W. Wang, W. J. Beuhler, S. J. Pickart, *J. Appl. Phys.* **1965**, *36*, 3232.
- [39] S. R. Butler, J. E. Hanlon, R. J. Wasilewski, *Met. Sci. J.* **1967**, *1*, 104.
- [40] D. P. Dautovich, Z. Melkvi, G. R. Purdy, C. V. Stager, *J. Appl. Phys.* **1966**, *37*, 2513.
- [41] R. J. Wasilewski, S. R. Butluer, J. E. Hanlon, D. Wordon, *Metall. Trans.* **1971**, *2*, 229.
- [42] M. Meier, C. Haberland, J. Frenzel, R. Zarnetta, in *Innovative Developments in Design and Manufacturing: Advanced Research in Virtual and Rapid Prototyping* (Eds: P. J. Bártolo, M. A. Jorge, H. A. Almeida, J. M. Matias, J. C. Vasco, J. B. Gaspar, M. A. Correia, N. C. Andre, N. F. Alves, P. P. Novo, P. G. Martinho, R. A. Carvalho), CRC Press, Taylor & Francis Group, Boca Raton, FL **2009**, p. 233.
- [43] P. Filip, K. Mazanec, *Scr. Mater.* **2001**, *45*, 701.
- [44] B. Tam, M. I. Khan, Y. Zhou, *Metall. Mater. Trans., A* **2011**, *42*, 2166.
- [45] M. Daly, A. Pequegnat, Y. Zhou, M. I. Khan, *Smart Mater. Struct.* **2012**, *21*, 045018.